iScience

CellPress
OPEN ACCESS

Article

Structural Diversity with Varying Disorder Enables the Multicolored Display in the Longhorn Beetle *Sulawesiella rafaelae*

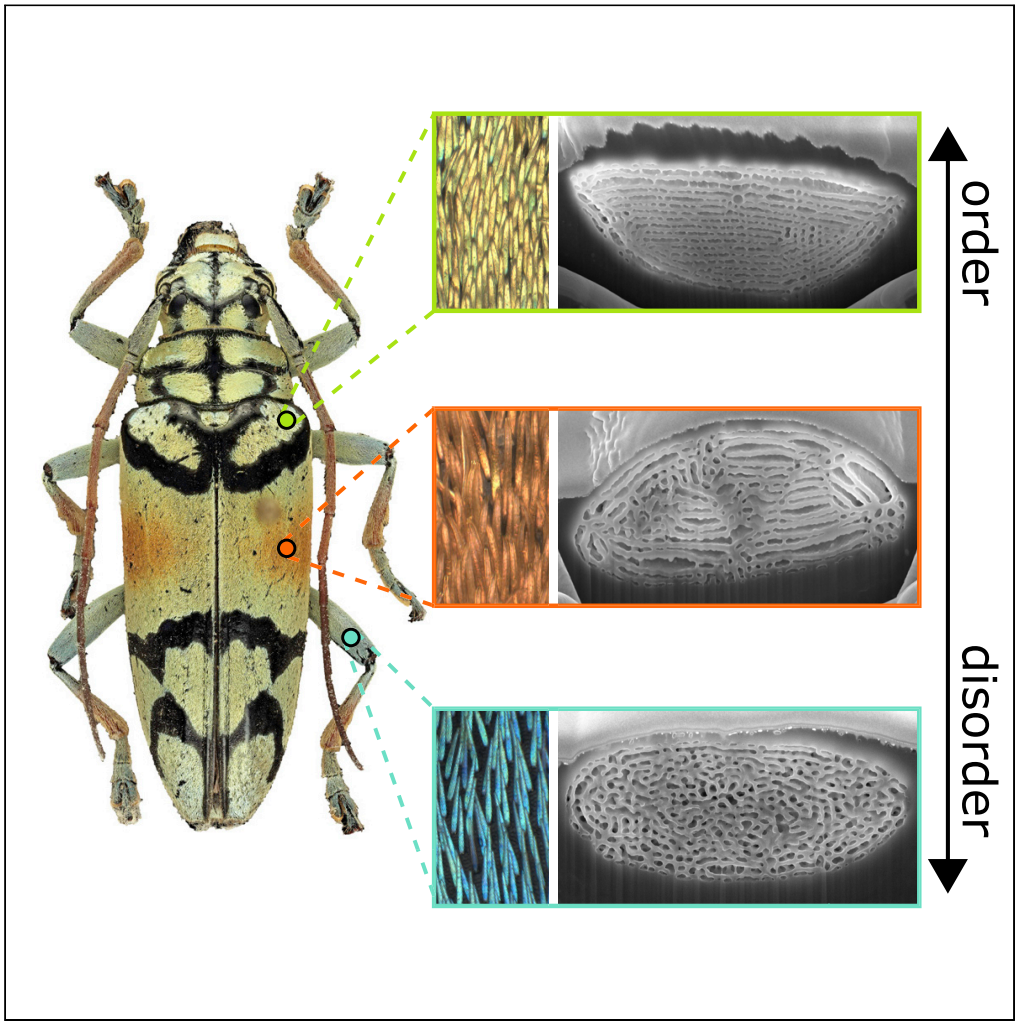

Esteban Bermúdez-Ureña, Cédric Kilchoer, Nathan P. Lord, Ullrich Steiner, Bodo D. Wilts

esteban.bermudez@unifr.ch (E.B.-U.)
bodo.wilts@unifr.ch (B.D.W.)

HIGHLIGHTS

The longhorn beetle *Sulawesiella rafaelae* features distinct body colors

The colors arise from interference of light at scales with different morphologies

A different degree of disorder results in different visual appearances

Bermúdez-Ureña et al., iScience *23*, 101339
July 24, 2020
https://doi.org/10.1016/j.isci.2020.101339

iScience

CellPress
OPEN ACCESS

Article

Structural Diversity with Varying Disorder Enables the Multicolored Display in the Longhorn Beetle *Sulawesiella rafaelae*

Esteban Bermúdez-Ureña,[1,*] Cédric Kilchoer,[1] Nathan P. Lord,[2] Ullrich Steiner,[1] and Bodo D. Wilts[1,3,*]

SUMMARY

Light control through layered photonic nanostructures enables the strikingly colored displays of many beetles, birds, and butterflies. To achieve different reflected colors, natural organisms mainly rely on refractive index variations or scaling of a fixed structure design, as opposed to varying the type of structure. Here, we describe the presence of distinct coloration mechanisms in the longhorn beetle *Sulawesiella rafaelae*, which exhibits turquoise, yellow-green, and orange colors, each with a variable iridescence. By optical and electron microscopy, we show that the colors originate from multilayered architectures in hair-like scales with varying amounts of structural disorder. Structural characterizations and optical modeling show that the disorder strongly influences the optical properties of the scales, allowing an independent adjustment of the optical response. Our results shed light on the interplay of disorder in multilayered photonic structures and their biological significance, and could potentially inspire new ecological research and the development of novel optical components.

INTRODUCTION

The huge diversity of colors encountered in nature arises mostly from pigmentary and structural coloration (Cott, 1940; Fox, 1976; Srinivasarao, 1999; Kinoshita, 2008), or a combination thereof. The combination of the pigmentary and structural coloration, i.e., by pigmentary doping of a nanostructure, allows a fine adjustment and filtering of the spectral response (Wilts et al., 2012; Vigneron et al., 2007; Teyssier et al., 2015). Such a combination of coloration strategies can be observed in many beetles, birds, and butterflies to produce their colorful displays (Stavenga, 2014; Seago et al., 2009). The visual, often highly patterned, display of an animal can serve important biological functions as diverse as communication, including signaling, mimicry and camouflage, warning coloration, or even non-visual functions, such as thermoregulation (Fox, 1976; Doucet and Meadows, 2009; Wilts et al., 2017a; Briscoe and Chittka, 2001; Cuthill et al., 2017), and the array of visual appearances is equally diverse. Many insects possess bold color patterns of a single-colored patch, likely to allow recognition, whereas many animals are multicolored, i.e., possess many different colored areas. In these multicolored animals, structural colors offer a big advantage compared with pigments thanks to their often narrow spectral response, which is determined by nanostructured architectures (Kinoshita and Yoshioka, 2005; Stavenga, 2014). Multicolor display strategies are also compatible with pigments, but they are restricted to subtractive colors, whereas structural color is innately additive.

Several strategies to exhibit multicolor displays have been identified in nature (Seago et al., 2009). In general, the reflected color is determined by the interference of light with dielectric structures of sub-wavelength dimensions (Kinoshita and Yoshioka, 2005; Srinivasarao, 1999), and color variations are usually achieved by modifying the interference conditions through scaling of the structure dimensions and/or variations in the effective refractive index. Probably the simplest strategy to generate color is via the interference of incident light in a single thin film. This can, for example, be observed in pigeon feathers (Yoshioka et al., 2007), fly wings (Stavenga, 2014), and the wing scales of *Micropterix* moths (Kilchoer et al., 2019b). In all these integumental structures, the minute control of the thin film thickness determines the animal's coloration. In the case of multilayer reflectors, the reflected hues are generally determined by controlling the thickness and periodicity of the constituent layers, as in the case of birdwing butterflies (Wilts et al., 2015; Zhang et al., 2014) and *Hoplia* beetles (Rassart et al., 2009; Kilchoer et al., 2019a), where a periodic

[1]Adolphe Merkle Institute, University of Fribourg, Chemin des Verdiers 4, 1700 Fribourg, Switzerland

[2]Department of Entomology, Louisiana State University Agricultural Center, 404 Life Sciences Building, LSU, Baton Rouge, LA 70803, USA

[3]Lead Contact

*Correspondence: esteban.bermudez@unifr.ch (E.B.-U.), bodo.wilts@unifr.ch (B.D.W.)

https://doi.org/10.1016/j.isci.2020.101339

arrangement of solid and nanoporous chitin layers is observed. Color variations are also possible in three-dimensional (3D) structures, where multiple parameters can be independently adjusted. For example, the rainbow coloration observed in *Pachyrrhynchus congestus* weevils is due to simultaneous changes in both the periodicity and the volume fill fraction of the 3D diamond nanostructure present in the elytral scales (Wilts and Saranathan, 2018). Note that coloration is typically described in terms of human perception and is often perceived differently by other organisms.

However, it is not only order that results in brilliant colored appearances. Similar principles exist for the color appearance of seemingly disordered nanostructures. As long as quasi-order is present, i.e., via a characteristic nearest-neighbor distance, dispartially ordered structures reflect colors that depend on their apparent periodicity and effective refractive index. Partially ordered nanostructures are encountered in bird feather barbs (Saranathan et al., 2012; Yin et al., 2012; Noh et al., 2010; Tinbergen et al., 2013), in damselflies (Veron et al., 1974; Prum et al., 2004; Henze et al., 2019), and in beetles (Dong et al. 2010, 2011; Pouya et al., 2011). Color variations stemming from structural diversity within the same organism are much less common, but have been documented in some beetle species (Saranathan et al., 2015). For example, in the *Eupholus magnificus* (Curculionidae) beetle (Pouya et al., 2011), the elytral scales present either highly ordered or quasi-ordered 3D photonic crystal structures, which cause the observed intense yellow and blue colors, respectively.

Here, we investigate the origin of the coloration of the longhorn beetle *Sulawesiella rafaelae* (Cerambycidae: Lamiinae: Tmesisternini), and show that hair-like, distinctly colored scales from different parts of the body act as multilayer-like reflectors, as a result of structurally diverse morphologies with different degrees of local disorder. The Tmesisternini tribe contains 12 genera and over 400 species, all with a distribution in Indo-Malaya, Southeast Asia, and the Australopacific geographic regions (Tavakilian and Chevillotte, 2018). The tribe and constituent genera and species were last thoroughly revised by Gressitt (1984), who remarked on the striking coloration of many of the members, as well as the tendency of species within and between closely related genera to form complex mimicry networks. Gressitt also discussed the high degree of color and pattern variability within species and/or between sexes. Tmesisternini species are diurnally active and strong flyers, although little about their natural history is known.

The genus *Sulawesiella* was erected for the species *Tmesisternus rafaelae*—one of the most spectacularly colored cerambycids (Figure 1) and a commonly traded specimen among collectors. The taxonomic placement of this species in a distinct genus from *Tmesisternus* (Weigel and Withaar, 2006) has not been comprehensively addressed and is based on a few characters that vary quite considerably, making identification challenging. *Sulawesiella* is monotypic, whereas the original genus, *Tmesisternus*, is the largest genus in the tribe (~330/400 species; Tavakilian and Chevillotte, 2018). The majority possess dull brown to black coloration, whereas several species possess striking iridescent pubescence (e.g., *Tmesisternus atrofasciatus*, *Tmesisternus cupreosignatus*, *Tmesisternus dohertyi*, *Tmesisternus elegans*, *Tmesisternus fulgens*, *Tmesisternus gabrieli*, *Tmesisternus insularis*, *Tmesisternus isabellae*, *Tmesisternus metalliceps*, *Tmesisternus ornatus*, *Tmesisternus salomonus*, *Tmesisternus schaumii*; see Gressitt, 1984; Weigel and Withaar, 2006).

S. rafaelae presented herein, has a strong resemblance in color appearance to its closely related species *T. isabellae* that has been previously investigated (Liu et al., 2009; Seo and Lee, 2017). Quite similarly to *T. isabellae*, *S. rafaelae* exhibits a metallic yellow-green color across its elytra and turquoise legs and antennae (Figure 1A). These previous studies only investigated scales from the elytra and attributed their color to a multilayer in the scale interior consisting of a homogeneous melanoprotein layer and an inhomogeneous layer composed of melanoprotein nanoparticles and air voids. In the case of the *S. rafaelae*, a clear difference with respect to *T. isabellae* is the presence of a dull orange patch located in the middle of the elytra (Figure 1A), which motivated us to have a closer look at the origin of the different colors observed in *S. rafaelae*. To the best of our knowledge, only the yellow-green scales of *S. rafaelae* have been briefly reported in a PhD thesis (Rassart, 2010).

RESULTS

Hair-like Scales Are Responsible for the Multicolored Display

The *S. rafaelae* specimens studied have an average length of 23 ± 4 mm and feature a multicolored appearance on both dorsal and ventral sides of the body. In dorsal view, the elytra (Figure 1A) exhibit a metallic yellow-green coloration covering the majority of the body, with prominent black patterns and dull orange patches breaking this coverage. The legs and the antennae have a turquoise optical appearance. Upon visual inspection at varying viewing angles, a prominent color change (i.e., iridescence) is noted

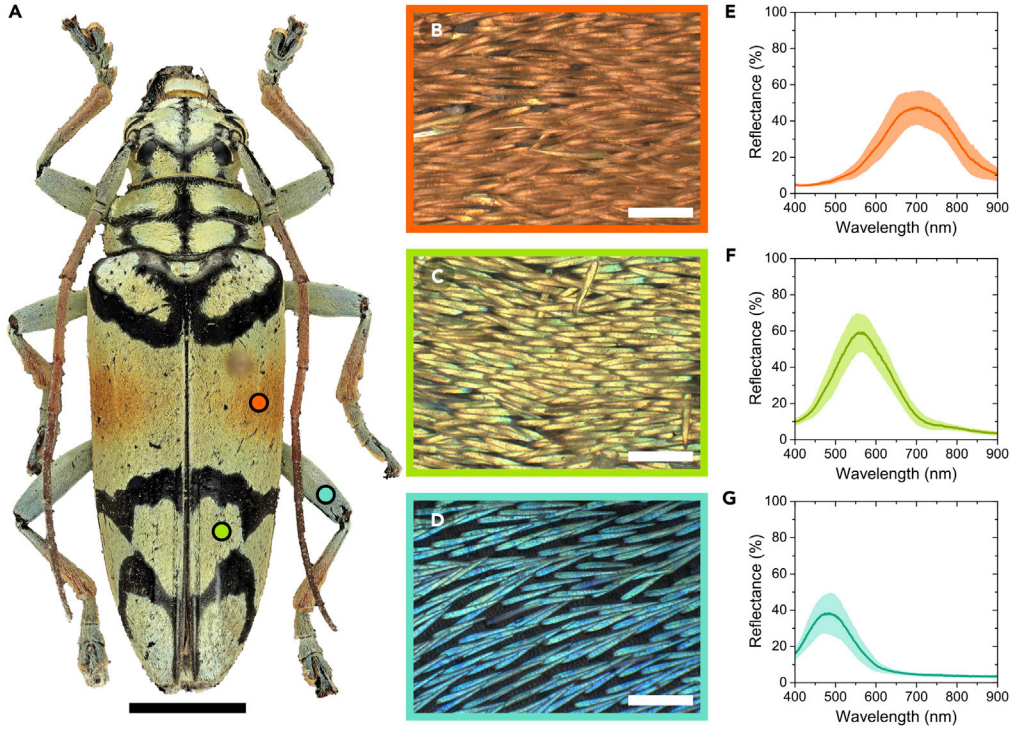

Figure 1. The Longhorn Beetle, *Sulawesiella rafaelae*

(A) Photograph of an adult specimen. The colored dots indicate the sampled areas.

(B–D) High-magnification micrographs of the scale arrangement in the different colored areas. The frame color corresponds to the dots in (A).

(E–G) Averaged reflectance spectra from multiple scales of the orange (E), yellow-green (F) and turquoise (G) regions, respectively, using a microspectrophotometer. For each region, ten scales were measured at five positions along the scale. The solid line corresponds to the mean value, and the shaded area indicates the standard deviation ($N = 50$). Scale bars: 5 mm in (A) and 20 μm in (B–D). See also Figure S1.

mainly for the yellow-green areas with a pronounced color change matching the turquoise appearance of the legs under high observation angles. A more subtle color shift is observed for the orange patches, whereas the turquoise color of the legs and antennae do not undergo a color shift with changing viewing angles. Optical microscopy showed that the color originates from elongated hair-like scales that are ~100 μm in length and ~10 μm in width (Figures 1B–1D). At such high magnification, the scales from each colored region can exhibit subtle variations in color on the single scale level.

To characterize the coloration of the scales, we collected multiple reflectance spectra from 10 representative scales from the orange, yellow-green, and turquoise regions using a microspectrophotometer (see Transparent Methods). The solid lines and shaded regions in Figures 1E–1G correspond to the mean and standard deviations of the collected spectra. Prominent reflectance bands are observed, with mean peak wavelengths centered at 707, 565, and 485 nm for the orange, yellow-green, and turquoise scales, respectively. The mean reflectance spectrum of yellow-green scales has a full width at half maximum (FWHM) of 159 nm and represents the brightest of the three scale types, with the turquoise scales having the lowest brightness levels and an FWHM of 131 nm. The orange scales have the broadest response with an FWHM of 206 nm. These spectral observations are in good accordance with the colors perceived by visual inspection. In the black areas, black-colored scales are also present above the otherwise black cuticle. These scales are similarly distributed as the scales at the colored regions, but with smaller dimensions (nearly 30% size reduction). Reflection spectra of the bare cuticle and from black scales reveal that the scales lower the overall reflectance to below 3% over the entire visible wavelength range (Figure S1).

To investigate the angle-dependent scattering properties of the scales, we performed back focal plane (*k*-space) imaging (Figures 2A–2C) of isolated scales by inserting a Bertrand lens into the collection pathway (Fu et al.,

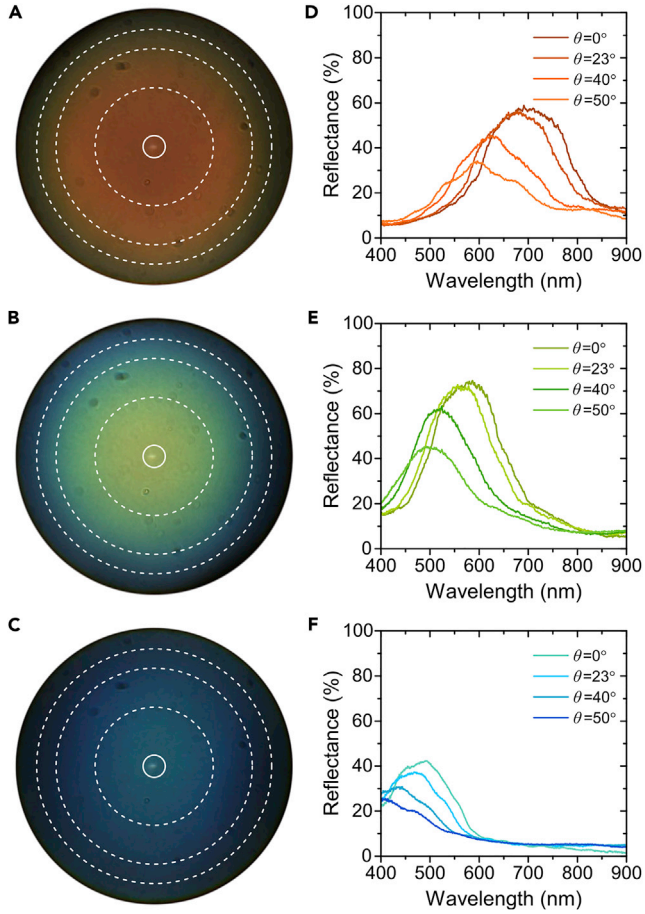

Figure 2. Light Scattering of Single Scales

(A–C) Back focal plane (*k*-space) imaging of representative individual orange, yellow-green, and turquoise scales. Measurements were done with an objective of 100×/NA 0.9, allowing to visualize scattering angles up to ~64°. The central solid line circle represents the size of the fiber collection spot, whereas the dashed line circles represent scattering angles of 23°, 40°, and 50°. NA, numerical aperture.

(D–F) Scattering spectra collected by displacing an optical fiber within the back focal plane images in (A–C), respectively. The fiber positions correspond to scattering angles of 0°, 23°, 40°, and 50°. Distinct blue-shifts of the reflection peaks are observed with increasing scattering angle.

2017). At first glance, the broad-angle illumination appears to show a more pronounced color change for the yellow-green scale (Figure 2B), followed by the orange and turquoise scales with more subtle apparent color variations (Figures 2A and 2C). Given that visual color shift is harder to perceive near the blue and red portions of the visible spectrum, to quantify the spectral shift as a function of scattering angle, we collected spectra at different positions within the back focal plane image, corresponding to scattering angles of 0°, 23°, 40°, and 50° (Figures 2D–2F). We measured three scales of each color, from which we extracted a relative peak wavelength shift of 95 $\pm$ 21 nm (orange), 80 $\pm$ 6 nm (yellow-green), and 67 $\pm$ 20 nm (turquoise) when the collected scattering angle transitioned from 0° to 50°. Although the orange scales exhibit a larger shift compared with the yellow-green scales at this microscopic level, this did not necessarily reflect in the perceived iridescence from the elytra at the macroscale. This can be associated to the broader spectral response of the orange scales and their reflectance being in the red portion of the visible spectrum, where color changes are harder to differentiate.

Scales Exhibit Multi-layer-type Structures with Varying Disorder

The reflectance spectra and scattering profiles indicate a structural origin of the observed coloration. To confirm this, we performed focused ion beam (FIB) and scanning electron microscopy (SEM) to image cross sections of representative colored scales (Figures 3A–3C and S2). Additional structural information from the 2D profiles was obtained by a layer orientation distribution analysis (Rezakhaniha et al., 2012) (Figures

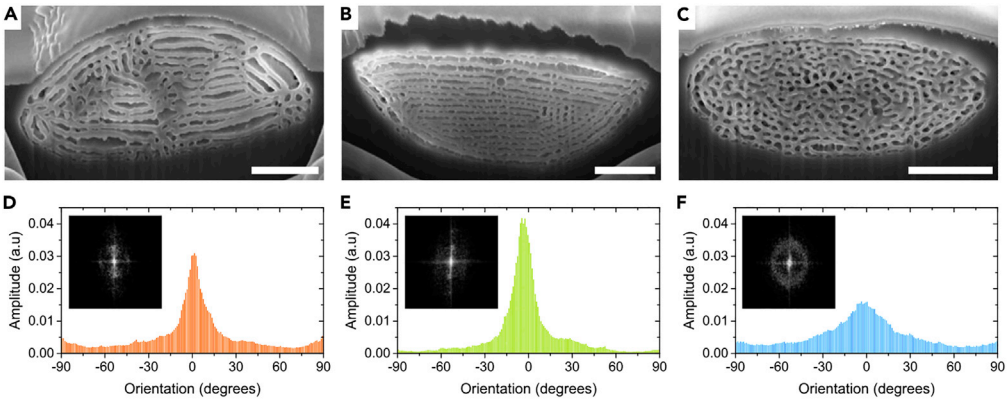

Figure 3. Ultrastructure of Single-Colored Scales

Cross-sectional SEM images and corresponding layer orientation distribution histograms of the ultrastructures associated with the (A and D) orange, (B and E) yellow-green, and (C and F) turquoise scales. The insets in (D–F) show the FFT of each scale. Scale bars, 2 μm (A–C). See also Figure S2.

3D–3F), as well as a fast Fourier transform (FFT) analysis to retrieve structural parameters (insets in Figures 3D–3F).

The orange (Figures 3A and 3D) and yellow-green (Figures 3B and 3E) elytral scales feature visually ordered multilayered structures, consisting of chitin layers spaced by layers that predominantly contain air (Liu et al., 2009). The level of layer ordering is confirmed by the histograms obtained from the layer orientation distribution analysis that shows narrow distributions around the horizontal in-plane orientation for both scales (Figures 3D and 3E). The yellow-green scales exhibit a higher degree of alignment than the orange scales, exhibiting larger amplitudes around the main angle orientation and lower contributions to the baseline at angles beyond $\pm 60°$. The latter could be responsible for the brighter and narrower reflectance response of the yellow-green scales when compared with the neighboring orange scales (Figures 1E and 1F). Looking across a central line through the scale's cross sections (Figure S2), we account for roughly 14 and 16 layers for the orange and yellow-green scales, respectively. Image analysis via FFT shows that the chitin layers have a spacing of 270 ± 35 nm and a chitin layer thickness of 127 ± 9 nm for the orange scale, and a spacing of 225 ± 28 nm and a layer thickness of 103 ± 7 nm for the yellow-green scale. This is in good accordance with the observed difference in human perceived coloration of the scales, because a reduction in layer thickness/periodicity is expected to blueshift a multilayer response (Stavenga et al., 2011; Kinoshita, 2008). Structural variations are considerable in these scales, which, along with the disorder introduced in the orientation of the layers, can contribute to the spread observed in the reflection bands of these scales (Figures 1E and 1F).

The turquoise scales (Figures 3C and 3F) vary considerably in ultrastructure compared with the other scales. In the turquoise scales, the multilayered structure seems to be absent. The lumen of the scale is rather filled with a disordered network of chitin struts and air. The higher degree of disorder compared with the orange and yellow-green scales is confirmed by a significantly broader distribution of structural orientations (Figure 3F). FFT analysis confirms this by showing an isotropic ring, in contrast to the aligned spots of the more ordered multilayers (Figures 3D and 3E). Instead of extracting a repetition unit of a multilayer, this ring allows to extract the mean repeat distance and strut thickness. For the turquoise scales, the chitin layer thickness is 85 ± 7 nm with a main repeat length of 183 ± 32 nm.

Scales Are Pigmented

To investigate the potential contribution of pigments to the observed colors, we reduced the refractive index variations in the scale material by using refractive-index-matching fluid with a refractive index of 1.55. Figure S3 shows that all scales contain broadband-absorbing pigments in the scales, reminiscent of melanin in the turquoise and yellow-green scales. The orange scales, in addition, contain a blue-absorbing pigment of unknown nature (absorbance peak at around 440nm), leading to a more pronounced absorption profile compared with the other scales.

Realistic Optical Modeling Using Finite-Difference Time-Domain Simulations

To verify the optical response arising from the seemingly different inner structures of the three colored scales, we first performed finite-difference time-domain (FDTD) optical modeling (see Transparent Methods). Figures 4A–4C show the FDTD results for the orange, yellow-green, and turquoise scales, respectively, with the solid lines and shaded areas corresponding to the mean and standard deviation for $N = 5$. For a simple comparison to the experiment, we plot selected spectra from the $N = 50$ measurements of Figures 1E–1G as non-shaded lines. Considering our simplified simulation, limited to normally incident light and averaging just over five cross sections within short ~1 μm segments, the FDTD results are in good agreement with representative experimental observations, both in the position of the reflection maxima and the relative intensities.

To emphasize the significance of performing such FDTD simulations with realistic profiles of the disordered ultrastructures, we also implemented an analytical transfer matrix method to model the optical response of idealized chitin/air multilayers (see Transparent Methods). The results for the orange, yellow-green, and turquoise scales are shown in Figures 4A–4C (dashed lines). For each type of scale, the reflection spectra correspond to the average of 100 generated multilayers with randomly assigned layer thicknesses. Although the position of the reflection maxima agree well with both experimental and 2D FDTD results (Figures 1 and 4 respectively), the expected intensities are much higher, resembling bright distributed Bragg reflectors. Given that we are considering comparable scale thickness values and equally accounting for the presence of wavelength-selective absorbing pigments (i.e., the presence of a complex refractive index), we attribute the lower intensity in the FDTD results to the presence of disorder within the scales, in the form of variable layer orientations (Figures 3D–3F), which further spatially spreads and weakens the optical response.

DISCUSSION

Interplay of Order and Disorder Leads to Varying Iridescence of the Different Colored Regions

The multilayer reflectors in the investigated beetles fall well within previously described structural coloration mechanisms, although multilayer reflectors in hair-like scales are less common (see Introduction). In general, ordered, multilayered reflectors in insects are quite common and appear in the elytra of many beetles (Stavenga et al., 2011; Seago et al., 2009; Kinoshita and Yoshioka, 2005; Rassart et al., 2009) and the wing scales of butterflies and moths (Kinoshita and Yoshioka, 2005; Srinivasarao, 1999; Wilts et al., 2015). The scales of *S. rafaelae* follow the designs of previously established structures. As we demonstrate, the mean distance of a chitin/air photonic structure determines the final color of the scales—with larger repeat periods the more longer wavelength reflecting the scale is—as found in many other natural structures.

What makes the scales of *S. rafaelae* rather unique is the fact that the distinct color of the scales arise from a multilayer reflector with different degrees of disorder. The yellow-green and orange patches are due to scales with rather ordered multilayer reflectors of different periodicity, whereas the turquoise scales show no apparent order in the chitin network of their scales (Figure 3). The experimental results (Figures 1, 2, and 3), together with modeling that compares between realistic and more idealized structures (Figure 4), convincingly show that it is the local disorder that brings forward scales with strongly different visual appearances.

The perceived color of the yellow-green scales is very angle dependent, whereas the angle-dependent color change of the orange scales is less pronounced. The latter is likely due to a higher degree of disorder in the orientation of the inner layers (Figure 3), which broadens the spectral response of individual orange scales. The macroscopic arrangement of the scales on the elytron will further influence the visual appearance. In the yellow-green and orange patches, the scales are well aligned, which likely results in a more macroscopically ordered reflective structure for the yellow-green spots. In addition, the presence of an additional blue-absorbing pigment in the orange scales will likely influence the angle dependency (Figure S3). We hypothesize that such a pigment will "narrow" down the reflectance at shorter wavelengths and thereby suppress a strong color change at larger scattering angles and so reduce the observable iridescence, similar to birdwing butterfly scales (Wilts et al., 2015).

The disorder in the turquoise scales of *S. rafaelae* is a surprising twist to the optical structure in the other scales and results in a distinct optical appearance without a discernible angle dependency. Such a

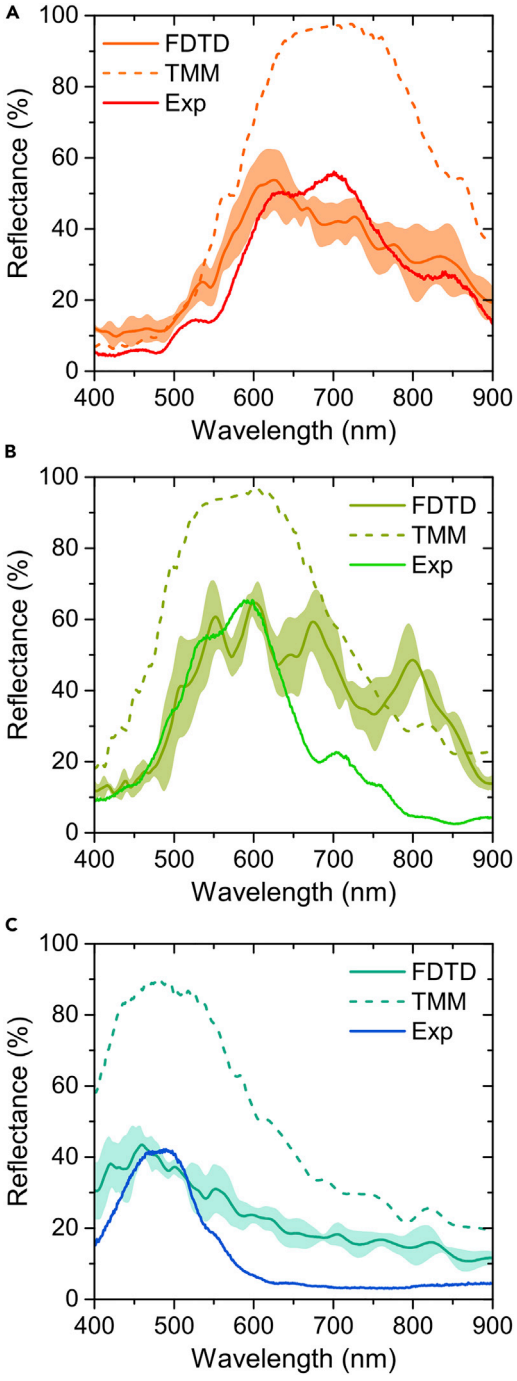

Figure 4. Optical Modeling

Simulated reflectance spectra based on a transfer matrix multilayer model (dashed lines) and 2D FDTD simulations using binary 2D profiles of the scale's cross sections (solid lines and shaded regions correspond to the mean and standard deviation, respectively, $N = 5$).

(A–C) Orange (A), yellow-green (B), and turquoise (C) scales. The non-shaded solid lines correspond to selected experimental spectra, accounted in Figures 1E and 1F, which have a good match to the FDTD results.

See also Figure S3.

difference in angle-dependent behavior for disordered or quasi-ordered structures has been seen before in other biological structures, as in the reflection gratings on the hair-like scales of peacock spiders (Wilts et al., 2020) or quasi-ordered networks of bird feather barbs (Noh et al., 2010; Tinbergen et al., 2013), and has also been employed in bio-inspired research to create angle-independent colors, e.g., by the random close-packed assembly of colloidal spheres (Forster et al., 2010) to synthesize photonic balls (Vogel et al., 2015). The macroscopic arrangement of scales with a disordered structure will effectively lower the iridescence observed at the single-hair level (Figure 2).

It is noteworthy that the chitin volume fraction of all scales of the investigated beetle is roughly similar, with ratios calculated from our FFT results of about 0.470, 0.457, and 0.464 for the orange, yellow-green, and turquoise scales, respectively, whereas the scale morphology and final scale size are quite different (Figures 1 and 3). It will be interesting to further investigate the assembly of these different morphologies from a developmental as well as a genetic viewpoint, as it is likely that the hair-like scales of *S. rafaelae* follow the general morphogenesis pathways as other insect structures (Ghiradella, 1989; Dinwiddie et al., 2014; Saranathan et al., 2015; Wilts et al., 2017b).

Biological Function of Color in Cerambycid Beetles

As described in the Introduction, the cerambycids are an incredibly speciose family (~35,000 described species; see Švácha and Lawrence, 2014; Tavakilian and Chevillotte, 2018) of phytophagous beetles with a worldwide distribution. Known as the longhorn beetles, the group gets its name for often extremely elongate antennae. Cerambycids have been shown to rely heavily on chemosensory stimuli for both host plant detection and mate recognition, and their elongated antennae likely play a critical role in compound detection (Hanks, 1999; Švácha and Lawrence, 2014). Although much work has been done on the chemical ecology of cerambycid beetles, far fewer investigations on the importance and prevalence of visual cues, specifically that of body coloration on inter- and/or intraspecific communication have been conducted.

Many cerambycids are nocturnal or crepuscular and dull brown or black in coloration, whereas there are numerous diurnal groups that are brightly colored by both pigmentary and structural mechanisms. Colors and patterns have been demonstrated to be critical to communication (especially sexual recognition and signaling) in myriad animal groups, but there is little evidence to suggest that visual recognition plays a pivotal role in cerambycid behavior.

Although bright colors have been shown to serve as an aposematic signal in some species of cerambycids (Seago et al., 2009), the presence of chemical defenses has not been broadly investigated across the group. Many of the colorful beetle taxa are involved in mimicry complexes with model species that are chemically defended (e.g., lycid beetles) or aggressive/defensive (e.g., Hymenoptera), and it is assumed that coloration serves primarily for crypsis or as an anti-predator defense (Švácha and Lawrence, 2014).

The investigated multicolored pattern of the *S. rafaelae* beetles is a good example, where nearly all visible colors can be observed (Figure 1). Along the elytra, the colored pattern is broken by the appearance of jet-black areas that strongly contrasts the multicolored patterns. As these areas are also carrying scales, the blackness is enhanced by black scales that are densely pigmented and show a highly disordered network structure in the lumen with irregular chitin features (see Figure S1). This disordered arrangement might work very similar to the "super-black" ornaments observed in other insects (Vukusic et al., 2004), arthropods (McCoy et al., 2019), and birds (McCoy and Prum, 2019), in absorbing reflected light and thereby enhancing the blackness of the otherwise more reflective black cuticle that is underlying the scales (see Figure S1). The distinct patterning of the *S. rafaelae* beetle may serve as disruptive signaling (Cuthill et al., 2005).

Conclusion

We investigated the distinctly multicolored scales of the longhorn beetle *Sulawesiella rafaelae*. Contrary to the more common approach of displaying multiple structural colors by varying the thickness and periodicity of the repeat units of a given type of structure alone, *S. rafaelae* exhibits a diverse set of structure morphologies with varying local order to achieve different color appearances throughout its body. Chitin-air multilayers are responsible for the colors observed on the elytra of the beetle with metallic yellow-green and orange appearance. The turquoise color of the scales on the legs arises instead from a disordered chitin-air network. The different degrees of disorder in these structures, manifested mainly by the presence

of segments with angled layers that cause the scales to diverge from an ideal parallel multilayer structure, are responsible for the different brightness levels as verified through optical modeling.

Although the iridescent colors and patterns found on these beetles may play a role in communication, the extreme intraspecific variability of these same colors and patterns and numerous instances of interspecific mimicry suggest they may not be of critical importance in recognition. Due to the diurnal nature of these beetles and presumably limited color visual systems, it is likely that the iridescent display and black patterns play a stronger role in crypsis or predator avoidance. The phylogenetic relatedness of iridescent taxa within the Tmesisternini (and Coleoptera as a whole), especially in contrast with the more common, predominantly drab-colored species, the function of these colors, and their production and maintenance in populations are interesting areas for further study. The implementation of structural diversity to generate different colors across the body is intriguing and needs further investigation into the *in vivo* mechanism underlying their synthesis. An insight into this complex structure formation not only will be interesting from a biological perspective but also might inspire the synthesis of optical structures with varying color and angle-dependent response.

Limitations of the Study

Our structural analysis as well as the optical modeling was limited to 2D cross sections of a beetle genus. However, deeper understanding of the extent of disorder throughout the scales could be obtained from a 3D analysis from the FIB-SEM cross sections. Similarly, optical simulations on a 3D model could provide additional insights into the angular-dependent response of the scales. An analysis of the extent of this phenomenon to related beetle families and the investigation of color polymorphism will be interesting to learn about potential selection pressures that have led to this development.

Resource Availability

Lead Contact

Further information and requests for resources and reagents should be directed to and will be fulfilled by the Lead Contact, Bodo Wilts (bodo.wilts@unifr.ch).

Materials Availability

This study did not generate new unique reagents.

Data and Code Availability

Original data have been deposited to Zenodo: https://doi.org/10.5281/zenodo.3909579.

METHODS

All methods can be found in the accompanying Transparent Methods supplemental file.

SUPPLEMENTAL INFORMATION

Supplemental Information can be found online at https://doi.org/10.1016/j.isci.2020.101339.

ACKNOWLEDGMENTS

We thank Prof. Doekele Stavenga and three reviewers for constructive comments on the manuscript. This work was financially supported by the Swiss National Science Foundation (163220, 168223), through the National Center of Competence in Research *Bio-inspired Materials*, the Adolphe Merkle Foundation, and the National Science Foundation (NSF DEB 1841704). This project has received funding from the European Union's Horizon 2020 Research And Innovation Programme under the Marie Skłodowska-Curie grant agreement No. 741855 and the ERC Advanced Grant agreement No. 833895.

AUTHOR CONTRIBUTIONS

Conceptualization: E.B.-U., C.K., and B.D.W.; Methodology: E.B.-U., C.K., and B.D.W., Investigation: E.B.-U., C.K., and B.D.W.; Writing – Original Draft: E.B.-U., C.K., and B.D.W.; Writing – Review and Editing: N.P.L. and U.S.; Resources: N.P.L.; Visualization: E.B.-U.; Funding Acquisition: E.B.-U., U.S., and B.D.W.

DECLARATION OF INTERESTS

The authors declare no conflicts of interest.

Received: May 3, 2020
Revised: June 24, 2020
Accepted: June 30, 2020
Published: July 24, 2020

REFERENCES

Briscoe, A.D., and Chittka, L. (2001). The evolution of color vision in insects. Annu. Rev. Entomol. *46*, 471–510.

Cott, H.B. (1940). Adaptive Coloration in Animals (Methuen & Co., Ltd).

Cuthill, I.C., Allen, W.L., Arbuckle, K., Caspers, B., Chaplin, G., Hauber, M.E., Hill, G.E., Jablonski, N.G., Jiggins, C.D., Kelber, A., et al. (2017). The biology of color. Science *357*, eaan0221.

Cuthill, I.C., Stevens, M., Sheppard, J., Maddocks, T., Párraga, C.A., and Troscianko, T.S. (2005). Disruptive coloration and background pattern matching. Nature *434*, 72–74.

Dinwiddie, A., Null, R., Pizzano, M., Chuong, L., Krup, A.L., Tan, H.E., and Patel, N.H. (2014). Dynamics of F-actin prefigure the structure of butterfly wing scales. Dev. Biol. *392*, 404–418.

Dong, B.Q., Liu, X.H., Zhan, T.R., Jiang, L.P., Yin, H.W., Liu, F., and Zi, J. (2010). Structural coloration and photonic pseudogap in natural random close-packing photonic structures. Opt. Express *18*, 14430–14438.

Dong, B.Q., Zhan, T.R., Liu, X.H., Jiang, L.P., Liu, F., Hu, X.H., and Zi, J. (2011). Optical response of a disordered bicontinuous macroporous structure in the longhorn beetle *Sphingnotus mirabilis*. Phys. Rev. E *84*, 011915.

Doucet, S.M., and Meadows, M.G. (2009). Iridescence: a functional perspective. J. R. Soc. Interfaces *6*, S115–S132.

Forster, J.D., Noh, H., Liew, S.F., Saranathan, V., Schreck, C.F., Yang, L., Park, J.-G., Prum, R.O., Mochrie, S.G., O'Hern, C.S., et al. (2010). Biomimetic isotropic nanostructures for structural coloration. Adv. Mater. *22*, 2939–2944.

Fox, D.L. (1976). Animal Biochromes and Structural Colours: Physical, Chemical, Distributional & Physiological Features of Coloured Bodies in the Animal World (University of California Press).

Fu, J., Yoon, B.-J., Park, J.O., and Srinivasarao, M. (2017). Imaging optical scattering of butterfly wing scales with a microscope. Interface Focus *7*, 20170016.

Ghiradella, H. (1989). Structure and development of iridescent butterfly scales: lattices and laminae. J. Morphol. *202*, 69–88.

Gressitt, J.L. (1984). Systematics and biogeography of the longicorn beetle tribe *Tmesisternini*. Pac. Insects Monogr. *41*, 1–263.

Hanks, L.M. (1999). Influence of the larval host plant on reproductive strategies of cerambycid beetles. Annu. Rev. Entomol. *44*, 483–505.

Henze, M.J., Lind, O., Wilts, B.D., and Kelber, A. (2019). Pterin-pigmented nanospheres create the colours of the polymorphic damselfly *Ischnura elegans*. J. R. Soc. Interface *16*, 20180785.

Kilchoer, C., Pirih, P., Steiner, U., and Wilts, B.D. (2019a). Diffusive structural colour in *Hoplia argentea*. J. Exp. Biol. *222*, jeb213306.

Kilchoer, C., Steiner, U., and Wilts, B.D. (2019b). Thin-film structural coloration from simple fused scales in moths. Interface Focus *9*, 20180044.

Kinoshita, S. (2008). Structural Colors in the Realm of Nature (World Scientific).

Kinoshita, S., and Yoshioka, S. (2005). Structural colors in nature: the role of regularity and irregularity in the structure. ChemPhysChem *6*, 1442–1459.

Liu, F., Dong, B.Q., Liu, X.H., Zheng, Y.M., and Zi, J. (2009). Structural color change in longhorn beetles *Tmesisternus isabellae*. Opt. Express *17*, 16183–16191.

McCoy, D.E., McCoy, V.E., Mandsberg, N.K., Shneidman, A.V., Aizenberg, J., Prum, R.O., and Haig, D. (2019). Structurally assisted super black in colourful peacock spiders. Proc. R. Soc. B. *286*, 20190589.

McCoy, D.E., and Prum, R.O. (2019). Convergent evolution of super black plumage near bright color in 15 bird families. J. Exp. Biol. *222*, jeb208140.

Noh, H., Liew, S.F., Saranathan, V., Mochrie, S.G.J., Prum, R.O., Dufresne, E.R., and Cao, H. (2010). How noniridescent colors are generated by quasi-ordered structures of bird feathers. Adv. Mater. *22*, 2871–2880.

Pouya, C., Stavenga, D.G., and Vukusic, P. (2011). Discovery of ordered and quasi-ordered photonic crystal structures in the scales of the beetle *Eupholus magnificus*. Opt. Express. *19*, 11355–11364.

Prum, R.O., Cole, J.A., and Torres, R.H. (2004). Blue integumentary structural colours in dragonflies (Odonata) are not produced by incoherent Tyndall scattering. J. Exp. Biol. *207*, 3999–4009.

Rassart, M., Simonis, P., Bay, A., Deparis, O., and Vigneron, J.P. (2009). Scale coloration change following water absorption in the beetle *Hoplia coerulea* (Coleoptera). Phys. Rev. E *80*, 031910.

Rassart, M. (2010). Etude de matériaux hygrochromes d'origine naturelle et de structures colorantes multi-échelles, PhD thesis (University of Namur).

Rezakhaniha, R., Agianniotis, A., Schrauwen, J., Griffa, A., Sage, D., Bouten, C., van de Vosse, F., Unser, M., and Stergiopulos, N. (2012). Experimental investigation of collagen waviness and orientation in the arterial adventitia using confocal laser scanning microscopy. Biomech. Model. Mechanobiol. *11*, 461–473.

Saranathan, V., Forster, J.D., Noh, H., Liew, S.-F., Mochrie, S.G.J., Cao, H., Dufresne, E.R., and Prum, R.O. (2012). Structure and optical function of amorphous photonic nanostructures from avian feather barbs: a comparative small angle X-ray scattering (SAXS) analysis of 230 bird species. J. R. Soc. Interfaces *9*, 2563–2580.

Saranathan, V., Seago, A.E., Sandy, A., Narayanan, S., Mochrie, S.G., Dufresne, E.R., Cao, H., Osuji, C.O., and Prum, R.O. (2015). Structural diversity of arthropod biophotonic nanostructures spans amphiphilic phase-space. Nano Lett. *15*, 3735–3742.

Seago, A.E., Brady, P., Vigneron, J.-P., and Schultz, T.D. (2009). Gold bugs and beyond: a review of iridescence and structural colour mechanisms in beetles (Coleoptera). J. R. Soc. Interfaces *6*, S165–S184.

Seo, H.-B., and Lee, S.-Y. (2017). Bio-inspired colorimetric film based on hygroscopic coloration of longhorn beetles (*Tmesisternus isabellae*). Sci. Rep. *7*, 44927.

Srinivasarao, M. (1999). Nano-optics in the biological world: beetles, butterflies, birds, and moths. Chem. Rev. *99*, 1935–1962.

Stavenga, D.G. (2014). Thin film and multilayer optics cause structural colors of many insects and birds. Mater. Today Proc. *1*, 109–121.

Stavenga, D.G., Wilts, B.D., Leertouwer, H.L., and Hariyama, T. (2011). Polarized iridescence of the multilayered elytra of the Japanese jewel beetle, *Chrysochroa fulgidissima*. Phil. Trans. R. Soc. B *366*, 709–723.

Švácha, P., and Lawrence, J. (2014). "Handbook of Zoology, Arthropoda: Insecta". In Morphology and Systematics (Phytophaga), *Vol. 3*, R. Leschen and R. Beutel, eds. (Walter de Gruyter), pp. 77–177, Chap. 2.4 Cerambycidae Latreille, 1802.

Tavakilian, G., and Chevillotte, H. (2018). Titan: International Database on Worldwide Cerambycidae or Longhorn Beetles. Version 4.0 (Titan). http://titan.gbif.fr/index.html.

Teyssier, J., Saenko, S.V., Van Der Marel, D., and Milinkovitch, M.C. (2015). Photonic crystals cause active colour change in chameleons. Nat. Commun. *6*, 6368.

Tinbergen, J., Wilts, B.D., and Stavenga, D.G. (2013). Spectral tuning of Amazon parrot feather coloration by psittacofulvin pigments and spongy structures. J. Exp. Biol. *216*, 4358–4364.

Veron, J., O'Farrell, A., and Dixon, B. (1974). The fine structure of Odonata chromatophores. Tissue Cell *6*, 613–626.

Vigneron, J.P., Pasteels, J.M., Windsor, D.M., Vértesy, Z., Rassart, M., Seldrum, T., Dumont, J., Deparis, O., Lousse, V., Biró, L.P., et al. (2007). Switchable reflector in the Panamanian tortoise beetle *Charidotella egregia* (Chrysomelidae: Cassidinae). Phys. Rev. E *76*, 031907.

Vogel, N., Utech, S., England, G.T., Shirman, T., Phillips, K.R., Koay, N., Burgess, I.B., Kolle, M., Weitz, D.A., and Aizenberg, J. (2015). Color from hierarchy: diverse optical properties of micron-sized spherical colloidal assemblies. Proc. Natl. Acad. Sci. U S A *112*, 10845–10850.

Vukusic, P., Sambles, J., and Lawrence, C. (2004). Structurally assisted blackness in butterfly scales. Proc. R. Soc. B *271*, S237–S239.

Weigel, A., and Withaar, G. (2006). Notes on the taxonomy of the genera tmesisternopsis breuning, 1945 and Tmesisternus latreille, 1829 (Coleoptera, cerambycidae, Tmesisternini), with description of a new genus from sulawesi. J. Zool. Soc. Lond. Wallacea *2*, 67–71.

Wilts, B.D., Matsushita, A., Arikawa, K., and Stavenga, D.G. (2015). Spectrally tuned structural and pigmentary coloration of birdwing butterfly wing scales. J. R. Soc. Interfaces *12*, 20150717.

Wilts, B.D., Michielsen, K., De Raedt, H., and Stavenga, D.G. (2012). Iridescence and spectral filtering of the gyroid-type photonic crystals in *Parides sesostris* wing scales. Interface Focus *2*, 681–687.

Wilts, B.D., Otto, J., and Stavenga, D.G. (2020). Ultra-dense, curved, grating optics determines peacock spider coloration. Nanoscale Adv. *2*, 1122–1127.

Wilts, B.D., and Saranathan, V. (2018). A literal elytral rainbow: tunable structural colors using single diamond biophotonic crystals in *Pachyrrhynchus congestus* weevils. Small *14*, 1802328.

Wilts, B.D., Vey, A.J., Briscoe, A.D., and Stavenga, D.G. (2017a). Longwing (*Heliconius*) butterflies combine a restricted set of pigmentary and structural coloration mechanisms. BMC Evol. Biol. *17*, 226.

Wilts, B.D., Zubiri, B.A., Klatt, M.A., Butz, B., Fischer, M.G., Kelly, S.T., Spiecker, E., Steiner, U., and Schröder-Turk, G.E. (2017b). Butterfly gyroid nanostructures as a time-frozen glimpse of intracellular membrane development. Sci. Adv. *3*, e1603119.

Yin, H., Dong, B., Liu, X., Zhan, T., Shi, L., Zi, J., and Yablonovitch, E. (2012). Amorphous diamond-structured photonic crystal in the feather barbs of the scarlet macaw. Proc. Natl. Acad. Sci. U S A *109*, 10798–10801.

Yoshioka, S., Nakamura, E., and Kinoshita, S. (2007). Origin of two-color iridescence in rock dove's feather. J. Phys. Soc. Jpn. *76*, 013801.

Zhang, K., Zhou, S., Tang, Y., Wang, G., Zhou, H., Fan, T., and Zhang, D. (2014). Polarization sensitive color in iridescent scales of butterfly Ornithoptera. RSC Adv. *4*, 51865–51871.

iScience, Volume *23*

Supplemental Information

Structural Diversity with Varying Disorder Enables the Multicolored Display in the Longhorn Beetle *Sulawesiella rafaelae*

Esteban Bermúdez-Ureña, Cédric Kilchoer, Nathan P. Lord, Ullrich Steiner, and Bodo D. Wilts

Supplementary Figures

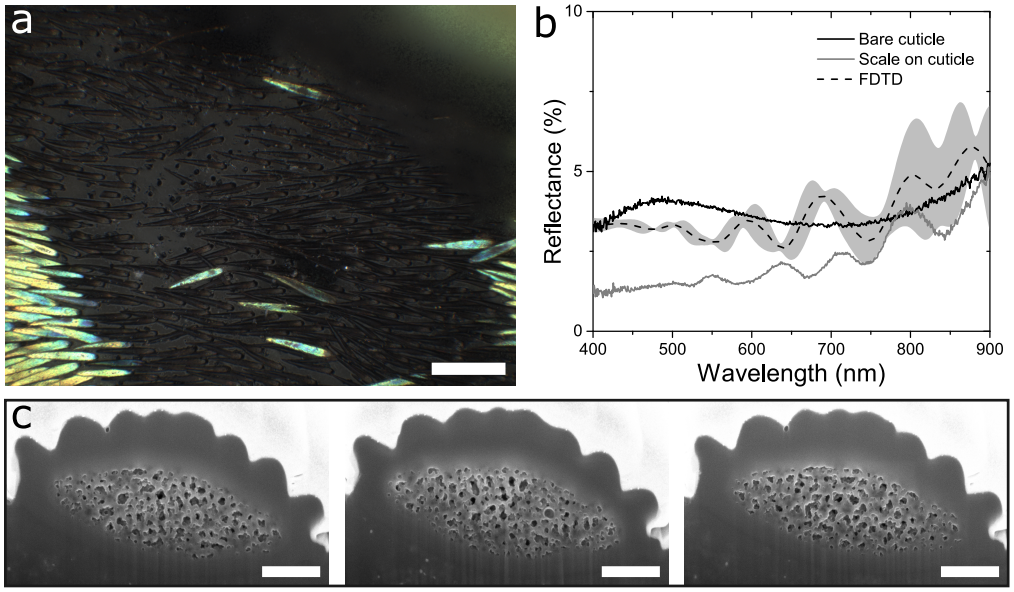

Figure S1. **Structure and optics of black scales, related to Figure 1.** a) Optical micrograph of a black region. Black scales are sparsely covering a dark brown elytra. b) Reflectance spectra for the bare cuticle surface (black solid line) and a scale above the cuticle (grey solid line). The mean and standard deviation of 2D FDTD simulated reflection spectra are shown as a black dashed line and shaded grey area respectively. c) FIB-SEM cross-section images of the black scale that were implemented to simulate the reflection spectra. Scale bars: a) 100 μm, c) 1 μm.

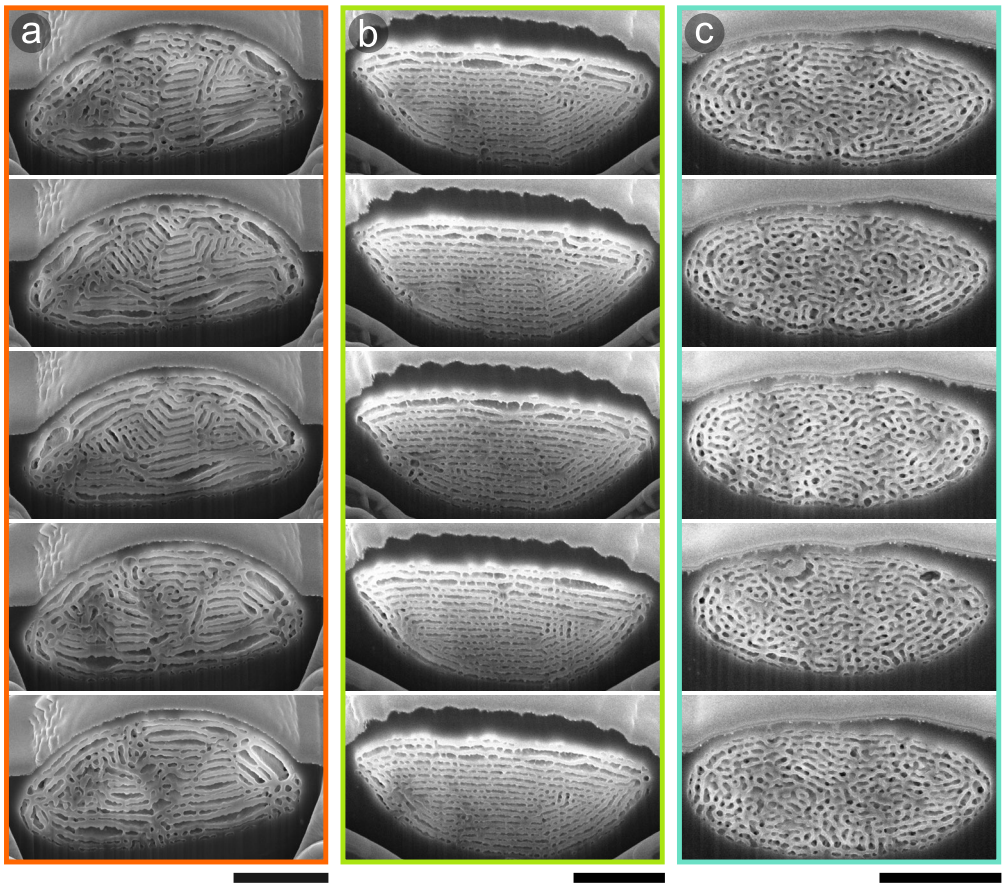

Figure S2. ***Sulawesiella rafaelae*** **scale cross-sections, related to Figure 3.** FIB-SEM cross-section images implemented in the FDTD simulations for the orange (a), yellow-green (b) and turquoise (c) colored scales. Scale bars: 3 µm

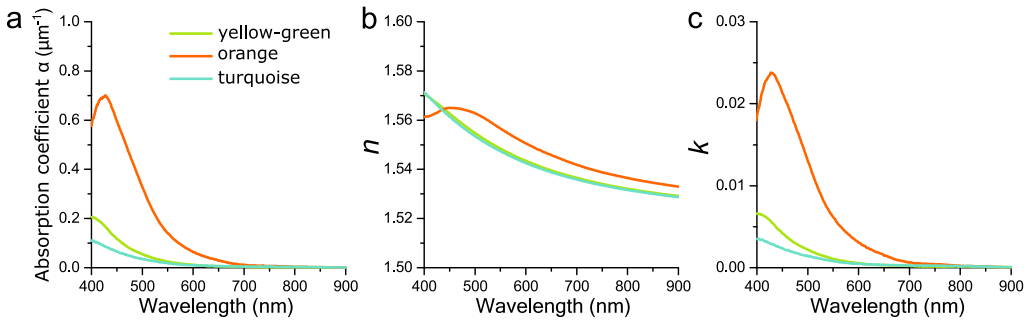

Figure S3. **Absorption and refractive indices, related to Figure 4.** a) Absorption coefficient α for orange, yellow-green, and turquoise colored scales derived from transmittance measurements of single wing scales immersed in refractive index-matching oil (see Transparent Methods). Real part (b) and imaginary part (c) of the refractive index $\tilde{n} = n + ik$ for the orange, yellow-green, and turquoise colored scales used in the FDTD modelling derived from Kramers-Kronig relations of the spectra shown in panel a.

Transparent Methods

Specimen

Specimen (N=13) of *Sulawesiella rafaelae* (Landsberge, 1885; Coleoptera: Cerambycidae: Lamiinae: Tmesisternini, Latreille, 1829) were purchased from Bughouse.be and insect-sale.com.

Optical characterization

Spectral characterization was performed using a xenon light source (Thorlabs SLS401; Thorlabs GmbH, Dachau, Germany) and a ZEISS Axio Scope.A1 microscope (Zeiss AG, Oberkochen, Germany) using an air objective (Zeiss Epiplan Apochromat 20x, NA 0.6). The light reflected from the sample was collected using an optical fibre (QP50-2-UV-BX, 50 µm core) with a measurement spot diameter ~4 µm. The spectra were recorded by a spectrometer (Ocean Optics Maya2000 Pro; Ocean Optics, Dunedin, FL, USA). Optical micrographs were captured with a CCD camera (GS3-U3-28S5C-C, Point Grey/ FLIR Integrated Imaging Solutions Inc., Richmond, Canada). k-space measurements were performed by placing a Bertrand lens (Zeiss 453671) into the imaging pathway and by using a high numerical aperture air objective (Zeiss Epiplan Neofluar 100x, NA 0 .9). This allows the measurement of scattering angles up to ~ 64°. The spectral measurements within the back focal plane image were recorded through an optical fiber (QP50-2-UV-BX). In all spectral measurements, a metallic mirror was used as a reference (Thorlabs PF10-03-P01).

Scale pigmentation

Isolated scales were immersed in a refractive-index matching fluid with a refractive index of 1.55 (Series A; Cargille Laboratories, Cedar Grove, USA). The absorbance of a scale was determined from a transmittance measurement *via* $A = -\log(T)$ and divided by the estimated effective solid thickness of the elytral scale (2.85 µm for green-yellow scales, 2.30 µm for orange scales and 2.05 µm for blue scales, estimated from FIB-SEM images). The refractive index dispersion spectra were calculated from the absorption coefficient by using Kramers-Kronig relations as detailed elsewhere (Wilts et al. 2017; Tianqi et al. 2020).

Ultrastructural analysis

Scales were detached from selected areas of the beetle and transferred to carbon adhesive discs glued onto standard SEM stubs (Plano-EM, Wetzlar, Germany). To prevent charging effects, a 5 nm gold layer was sputter coated on the samples (Cressington 208 HR, Cressington Scientific Instruments, Watford, England). Scale cross-sections were prepared and imaged using a FEI Scios 2 dual-beam scanning electron microscope equipped with a Ga^+ column and a field-emission electron gun (FEI, Eindhoven, the Netherlands).

Structural analysis of the SEM cross-sectional images was performed using Fiji (Schindelin et al. 2012). The OrientationJ plug-in (http://bigwww.epfl.ch/demo/orientation/) was used for the layer orientation analysis, on the image-processed and binarized 2D cross-sections, using a local window of ∼30 nm and minimum coherency and energy values of 5%. FFT analysis was also performed using Fiji's built-in FFT tool and structural length and mean layer thicknesses were extracted from the primary and secondary structural features of the FFT, respectively.

Optical modelling

Two-dimensional (2D) optical modelling was performed with a finite-difference time-domain (FDTD) method using commercial software (FDTD Solutions, v. 8.20; Lumerical Inc, Canada). We directly processed the cross-sections of Fig. 3, imported these as binary 2D profiles into our 2D FDTD simulation box and assigned calculated complex refractive index data for each type of scale (Fig. S3). For each colored scale, we averaged the simulated response of five different cross-sections extracted from the same scale within a $\sim$ 1 μm length (Fig. S2). In the 2D FDTD simulation, we considered unpolarized plane-wave illumination (400 – 900 nm), perfectly matched layers for all boundaries, and a mesh size of 5 nm. The width of the FDTD region was set to 4 μm, approximating the experimental collection spot size. Linear power monitors placed behind the source were used to collect the reflected power from the imported binary profiles.

In addition, we implemented an analytical transfer matrix method to model the optical response of idealized chitin/air multilayers (STACK solver, Lumerical Inc, Canada). In this method, for each of the three colored scales, we considered stacks of 15 chitin/air bilayers with randomly assigned thicknesses based on the mean and standard deviation values extracted from fast Fourier transform (FFT) analysis of SEM cross-sections. The presence of the enveloping cortex was also considered. For the material properties we used the same complex refractive index data as in the 2D FDTD simulations. The results in Figure 4 (dashed lines) correspond to the average over 100 iterations.

Supplementary References

Schindelin, J., Arganda-Carreras, I., Frise, E., Kaynig, V., Longair, M., Pietzsch, T., Preibisch, S., Rueden, C., Saalfeld, S., Schmid, B., et al. (2012) Fiji: an open-source platform for biological-image analysis. Nat. Methods. 9, 676–682.

Tianqi, S., Saba, M., Dufresne, E., Steiner, U., and Wilts, B. D. (2020) Designing Refractive Index Fluids using the Kramers-Kronig Relations. Faraday Discuss., doi: 10.1039/D0FD00027B.

Wilts, B. D., Wijnen, B., Leertouwer, H. L., Steiner, U., and Stavenga, D. G. (2017) Extreme refractive index wing scale beads containing dense pterin pigments cause the bright colors of pierid butterflies. Adv. Opt. Mater. 5, 1600879.